Loss of CRB2 in the mouse retina mimics human retinitis pigmentosa due to mutations in the CRB1 gene.

Celso Henrique Alves, Alicia Sanz Sanz, Bokyung Park, Lucie P. Pellissier, Naoyuki Tanimoto, Susanne C Beck, Gesine Huber, Mariyam Murtaza, Fabrice Richard, Iswariyaraja Sridevi Gurubaran, et al.

Loss of CRB2 in the mouse retina mimics human retinitis pigmentosa due to mutations in the *CRB1* gene

Celso Henrique Alves[1], Alicia Sanz Sanz[1], Bokyung Park[1], Lucie P. Pellissier[1], Naoyuki Tanimoto[3], Susanne C. Beck[3], Gesine Huber[3], Mariyam Murtaza[4], Fabrice Richard[5,6], Iswariyaraja Sridevi Gurubaran[1], Marina Garcia Garrido[3], Christiaan N. Levelt[2], Penny Rashbass[4], André Le Bivic[5,6], Mathias W. Seeliger[3] and Jan Wijnholds[1,*]

[1]Department of Neuromedical Genetics and [2]Department of Molecular Visual Plasticity, The Netherlands Institute for Neuroscience, Royal Netherlands Academy of Arts and Sciences (KNAW), Meibergdreef 47, 1105 BA Amsterdam, The Netherlands, [3]Division of Ocular Neurodegeneration, Institute for Ophthalmic Research, Centre for Ophthalmology, Eberhard Karls University of Tübingen, Tübingen D-72076, Germany, [4]University of Sheffield, Alfred Denny Building, Western Bank, S102TN Sheffield, UK, [5]Developmental Biology Institute of Marseille Luminy (IBDML), Aix-Marseille University (AMU) and [6]CNRS, UMR 6216, IBDML, Case 907, 13288 Marseille, Cedex 09, France

In humans, the Crumbs homolog-1 (*CRB1*) gene is mutated in progressive types of autosomal recessive retinitis pigmentosa and Leber congenital amaurosis. However, there is no clear genotype–phenotype correlation for *CRB1* mutations, which suggests that other components of the CRB complex may influence the severity of retinal disease. Therefore, to understand the physiological role of the Crumbs complex proteins, we generated and analysed conditional knockout mice lacking CRB2 in the developing retina. Progressive disorganization was detected during late retinal development. Progressive thinning of the photoreceptor layer and sites of cellular mislocalization was detected throughout the CRB2-deficient retina by confocal scanning laser ophthalmoscopy and spectral domain optical coherence tomography. Under scotopic conditions using electroretinography, the attenuation of the a-wave was relatively stronger than that of the b-wave, suggesting progressive degeneration of photoreceptors in adult animals. Histological analysis of newborn mice showed abnormal lamination of immature rod photoreceptors and disruption of adherens junctions between photoreceptors, Müller glia and progenitor cells. The number of late-born progenitor cells, rod photoreceptors and Müller glia cells was increased, concomitant with programmed cell death of rod photoreceptors. The data suggest an essential role for CRB2 in proper lamination of the photoreceptor layer and suppression of proliferation of late-born retinal progenitor cells.

INTRODUCTION

The establishment and maintenance of apical–basal polarization and adhesion is controlled by apical polarity protein complexes, which are crucial for proper lamination of mammalian photoreceptor cells (1–8). The apical Crumbs complex resides in the adult retina at a subapical region adjacent to adherens junctions between photoreceptors and Müller glia cells (2,9). In amniotes, there are four Crumbs family members, CRB1, CRB2, CRB3A and CRB3B (10). In zebrafish, the family consists of Crb1, Crb2a (Ome), Crb2b, Crb3a and Crb3b (11,12). The prototypic CRB protein has a large extracellular domain with epidermal growth factor and laminin-globular domains, a single transmembrane domain and a short 37 amino acid intracellular C-terminus containing single-FERM and -PDZ protein-binding motifs (13). The core proteins of the complex are either CRB–PALS1 (protein associated with Lin Seven 1)–PATJ (PALS1-associated tight junction

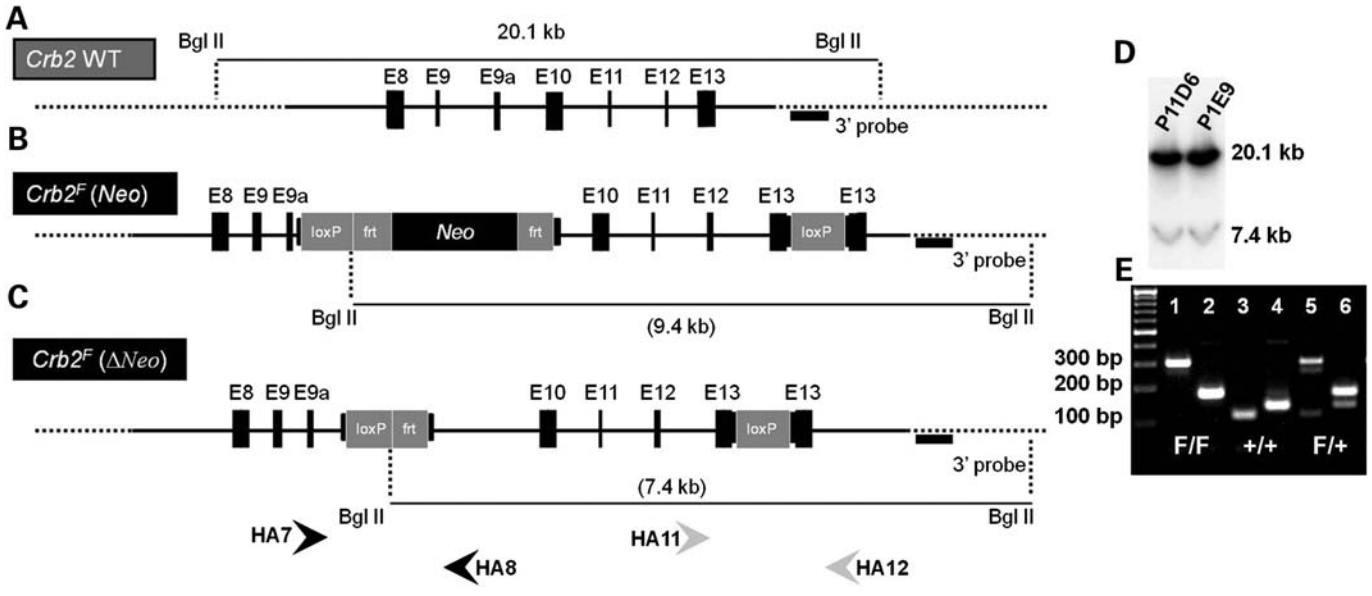

Figure 1. Schematic representation of the *Crb2* targeting construct and genotyping strategy. (**A**) *Crb2* WT gene composed of 13 exons. (**B**) *Crb2* targeting construct, the *loxP* recombination sites are located between exons 9a and 10, and in exon 13, in the 3′ untranslated region. The targeting construct also contains a neomycin cassette flanked by *frt* recombination sites. (**C**) *Crb2* targeting construct after *frt* recombination and deletion of the neomycin cassette. The localization of the 3′ end arm probe used to characterize the targeting construct, and of the pairs of primers, HA7/8 and HA11/12, located around the *loxP* recombination sites and used for genotyping, are represented in the figure. Two *Bgl*II restriction sites locate outside the targeted DNA; one extra *Bgl*II restriction site is present in the targeting construct near the 5′ end *loxP* site. (**D**) Southern blotting analysis of $Crb2^{F/+}$ embryonic stem-cell genomic DNA digested using *Bgl*II showed a 20.1 kb fragment corresponding to the WT allele and a 7.4 kb fragment corresponding to the *Crb2* floxed allele. (**E**) PCR genotyping of $Crb2^{F/F}$ (F/F), $Crb2^{+/+}$ (+/+) and $Crb2^{F/+}$ (F/+) mice. The left lane contains 100 bp DNA size markers, and the pairs of subsequent lanes contain PCR products of $Crb2^{F/F}$ (lanes 1 and 2), $Crb2^{+/+}$ (lanes 3 and 4) and $Crb2^{F/+}$ mouse DNA (lanes 5 and 6). Lanes 1, 3 and 5 contain the HA7/8 reaction product and the lanes 2, 4 and 6 contain the HA11/12 reaction product.

protein) or CRB–PALS1–MUPP1 (MUPP1—multi-PDZ domain protein 1) (2,14–18). The C-terminal PDZ motif of CRB interacts with the PDZ domain of PALS1, which in turn binds via an N-terminal L27 domain to the L27 domain of PATJ and MUPP1 (18). The PDZ motif of CRB can also interact with PAR6 (19), which can also bind to PALS1 (20). The multi-adaptor protein PALS1 recruits MPP3 and MPP4 into the apical complex (15,16). The FERM motif binds to EPB4.1L5, the mammalian homologue of *Drosophila* Yurt and zebrafish Mosaic Eyes (Moe) (21–23).

In humans, mutations have been identified in the *CRB1* gene in individuals with Leber congenital amaurosis, retinitis pigmentosa type 12, retinitis pigmentosa with Coats-like exudative vasculopathy and other early-onset retinitis pigmentosa (10,24,25). In the mouse retina, CRB1 maintains adherens junctions between photoreceptors and Müller glia cells and prevents retinal disorganization and dystrophy; moreover, the loss of CRB1 results in a phenotype limited to one retinal quadrant (1,2). However, the severity of the phenotype is strongly dependent on the genetic background, as different mutations in *CRB1/Crb1* cause various retinal phenotypes in human and mice. The lack of a clear genotype–phenotype correlation suggests that other components of the Crumbs complex have a function influencing the severity of the retinal disease. In zebrafish, the two *Crb2* genes (*Crb2a* and *Crb2b*) have been implicated in retina developmental and morphological defects. Crb2a (Ome) is a determinant of apicobasal polarity in the retina, and the loss of Crb2a causes severe basal displacement of cell junctions in neuroepithelial cells (11,12). *Ome* mutants display gross morphological abnormalities of the retina with inappropriate lamination and ectopic apical surfaces (26). Moreover, zebrafish Crb2b is essential for the determination of the size of apical membrane domain within photoreceptors. Overexpression of mouse *Crb2* in embryonic stem cells increased cell proliferation and reduced terminal neural differentiation (27).

Here, we study the effects of the loss of CRB2 from the developing mouse retinal neuroepithelium. Our findings show that conditional deletion of *Crb2* in the retina results in early retinal disorganization leading to severe and progressive retinal degeneration with a concomitant visual loss that mimics retinitis pigmentosa due to mutations in the *CRB1* gene, and suggest a role for CRB2 in suppressing proliferation of late retinal progenitors.

RESULTS

Lack of CRB2 impairs retinal function in adult mice

In mice, the degeneration due to the loss of CRB1 is limited to one quadrant of the retina, suggesting compensatory mechanisms (2). To ablate CRB2 function in the mouse, *loxP* sites were inserted in the *Crb2* gene between exons 9a and 10 and in exon 13 downstream of the stop codon (Fig. 1). *Crb2* floxed homozygous ($Crb2^{F/F}$) mice showed no identifiable phenotype, had a normal lifespan and were fully fertile. We crossed the *Crb2* conditional knockout (cKO) with Chx10-*Cre* mice to obtain *Crb2*Chx10 cKO ($Crb2^{F/F}/Chx10Cre^{+/-}$)

animals. Chx10-*Cre* drives Cre-mediated recombination in neuroepithelial progenitors of the retina (28), resulting in the loss of CRB2 expression at the apical surface from embryonic day (E) 12.5 (Supplementary Material, Fig. S1).

We performed functional and structural *in vivo* analyses of 1–18-month-old *Crb2*Chx10 cKO and control mice, using electroretinography, spectral domain optical coherence tomography and scanning laser ophthalmoscopy. In electroretinography experiments under both scotopic and photopic conditions, there was no significant difference between the control animals ($Crb2^{F/+}/Chx10Cre^{+/-}$ and $Crb2^{F/F}$) mice at any of the time points analysed (Fig. 2A–C). In contrast, already 1-month-old *Crb2*Chx10 cKO mice showed considerable reduction in amplitudes of both scotopic and photopic electroretinography responses, indicating alterations of both rod and cone system components (Fig. 2A). At high stimulus intensities under scotopic conditions, the attenuation of the a-wave was relatively stronger than that of the b-wave (Fig. 2A), resulting in a high b/a ratio (Fig. 2B). As the initial portion of the a-wave reflects the primary light response in photoreceptors, the remarkable attenuation of the a-wave observed in *Crb2*Chx10 cKO mice indicates a strong photoreceptor dysfunction. Furthermore, in *Crb2*Chx10 cKO mice, the signal amplitudes progressively decreased with age, until they became practically extinguished around 18 months of age (Fig. 2C).

In the *in vivo* imaging analysis using scanning laser ophthalmoscopy and spectral domain optical coherence tomography, control littermates did not show any abnormalities in fundus appearance, fundus autofluorescence, retinal vasculature and retinal morphology at any time point. Also, no differences were observed between the $Crb2^{F/+}/Chx10Cre^{+/-}$ and $Crb2^{F/F}$ mice (Fig. 3A–E). In contrast, 1-month-old *Crb2*Chx10 cKO retinae revealed changes in fundus appearance as well as in retinal layer morphology, suggesting a progressive retinal degeneration (Figs 3F–J and 4A–O). With native scanning laser ophthalmoscopy, many spots and patchy areas were visible, and fundus autofluorescence revealed accumulation of autofluorescent remains from lost photoreceptor cells. Commonly, degenerative processes are characterized by accumulation of autofluorescent material, mainly break-down products of photoreceptor outer segments that contain the visual pigment chromophore 11-*cis* retinal, in the retina (29). These data were supported by spectral domain optical coherence tomography analysis. A significant reduction of retinal thickness, compared with control animals, was found in the outer retina of *Crb2*Chx10 cKOs. Furthermore, sites with cellular mislocalization were detected (Fig. 4D and I and insets E and J). In the *Crb2*Chx10 cKOs, a further progression of the retinal degeneration was observed (Fig. 4A, F and K). Most severe degeneration was found, particularly in the central retina surrounding the optic disc and at sites of cellular mislocalization.

Additionally, in the *Crb2*Chx10 cKO, the retinal vasculature was affected already at 3 months of age (Fig. 4C). With fluorescein angiography (FLA), sites of neovascularization were observed very similar to vascular abnormalities detected in $Crb1^{-/-}$ mice (3). At some of these sites (Fig. 4H and M), choroidal structures were visible, suggesting disruption of the retinal pigment epithelium layer. These processes were clearly visualized by spectral domain optical coherence tomography imaging (Fig. 4E, J and O). Taken together, our results indicate that *Crb2*Chx10 cKO animals have a strong retinal phenotype with severe functional consequences.

CRB2 is required in retinal development

The *in vivo* studies suggested abnormalities during retinal development. CRB2 is localized at E11.5 in retinal progenitor cells (Supplementary Material, Fig. S1) and later on in photoreceptors and Müller glia cells (30). Morphological alterations in the *Crb2*Chx10 cKO were found from E18.5 (Figs 5B and 6D and F). In the *Crb2*Chx10 cKO, sporadic disruptions of the outer limiting membrane and mislocalized cell nuclei in the subretinal space were observed at the periphery of the retina (Figs 5B and 6D and F). The *Crb2*Chx10 cKO lost CRB2 expression from the subapical region (Fig. 6B and Supplementary Material, Fig. S1) and displayed disrupted adherens junctions and subapical region (Fig. 6D, F, H, J, L and N).

At postnatal day (P) 3, the *Crb2*Chx10 cKO retinal progenitors and newly born photoreceptors had lost their normal orientation and instead formed rosettes and half-rosettes at the periphery of the retina (Fig. 5D). These rosettes consisted of immature retinal cells with adherens junctions and subapical regions positive for apical proteins such as MUPP1 and PATJ (Supplementary Material, Fig. S2D–F). Recoverin is a marker for immature as well as mature photoreceptors and some cone bipolar cells, and in regions where the adherens junctions were disrupted, recoverin-positive cells were displaced from the apical surface and localized ectopically in the centre of the neuroepithelial layer (Fig. 7B). Moreover, we observed an increase in the number of recoverin-positive cells in the *Crb2*Chx10 cKO compared with the control (24.0 ± 0.6 versus 21.9 ± 0.4 recoverin-positive cells/100 μm $\pm$ SEM; Supplementary Material, Fig. S3). In addition, we observed, near these rosettes, ectopic nuclei of cells in the subretinal space adjacent to the adherens junctions (Fig. 5D).

At P6, rosettes and half-rosette structures could also still be observed at the periphery of the retina. Interestingly, the rosettes contained cells positive as well as negative for the proliferation markers phospho-histone H3 (pH3), Ki67 and apical marker PATJ (which marks the apical membrane but also co-stains a subset of Ki67-positive cells at the periphery of the developing retina) (Fig. 8D). In addition, ectopic nuclei were detected in the subretinal space throughout the retina. These were situated both alone or in small clusters (Fig. 5F and 7D). Some of these nuclei were positive for recoverin but negative for rhodopsin (a marker for mature rod photoreceptors), and others were positive for both recoverin and rhodopsin (Fig. 7D). Transmission electron microscopy showed local loss of adherens junctions near these ectopic cells (Fig. 9B).

At P10, the outer limiting membrane was disrupted throughout the mutant retina. These disruptions lead to an increased number of ectopic nuclei residing in the subretinal space immediately adjacent to the retinal pigment epithelium (Fig. 5H and 7F and H; Supplementary Material, Fig. S4B). Most of these cell bodies were positive for recoverin (Fig. 7F) and rhodopsin (Fig. 7H). The ectopic photoreceptors in the subretinal space did not develop proper segments, implying that these cells were immature non-polarized

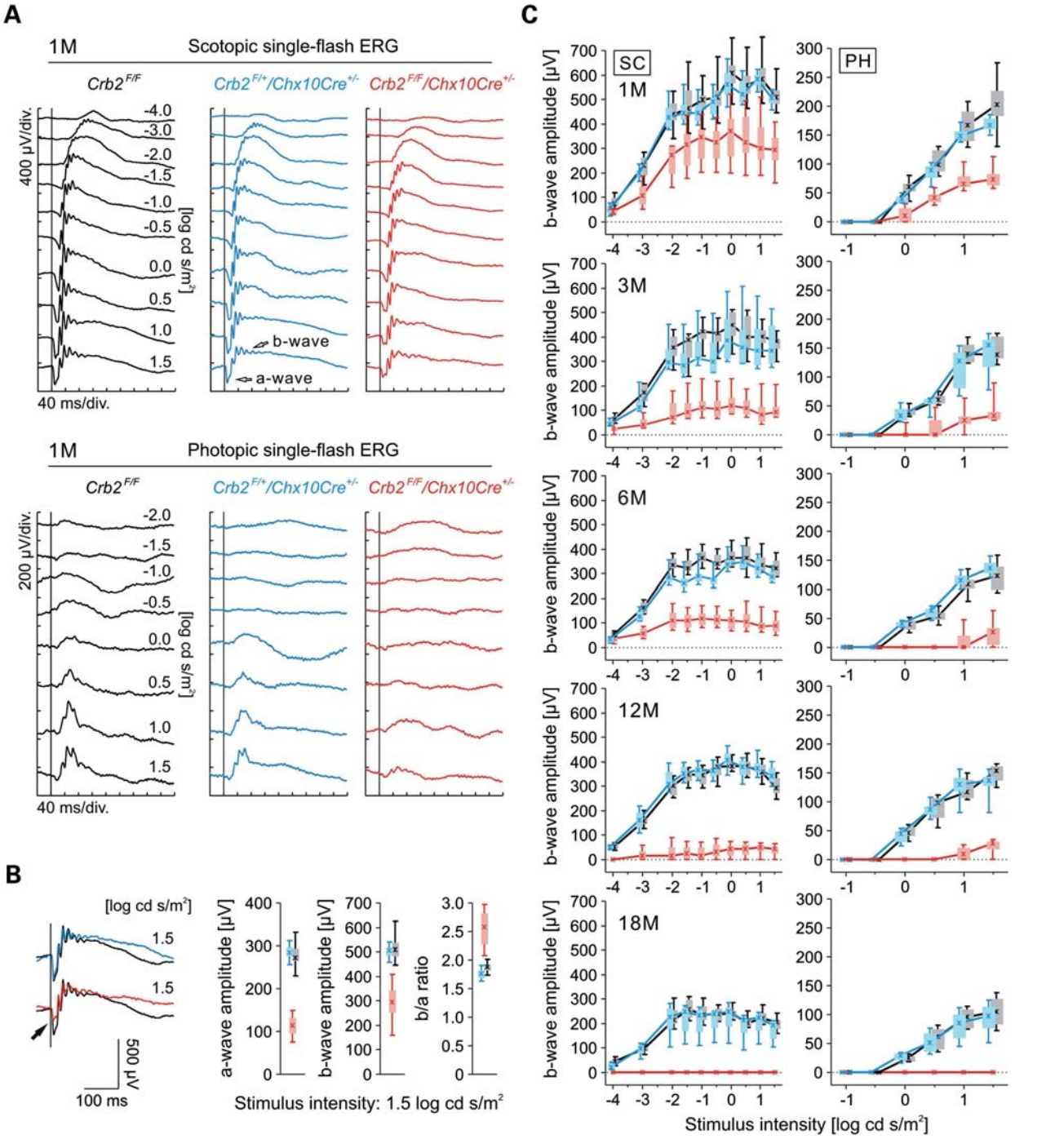

Figure 2. Progressive loss of retinal function in *Crb2*Chx10 cKO animals *in vivo*. Electroretinographic time course of retinal function in $Crb2^{F/F}$ control (black), $Crb2^{F/+}/Chx10Cre^{+/-}$ heterozygous (blue) and $Crb2^{F/F}/Chx10Cre^{+/-}$-affected mice (red). (**A**) Scotopic (top) and photopic (bottom) single-flash electroretinography responses from representative animals at the age of 1 month. The a-wave and the b-wave are indicated by open arrows. (**B**) Left: Superposition of scotopic single-flash electroretinography responses (1.5 log cd s/m^2) from (A). The arrow points to the attenuated a-wave of the affected mouse. Right: Quantitative evaluation of scotopic single-flash a-wave and b-wave amplitudes (1.5 log cd s/m^2) as well as the corresponding b-wave/a-wave amplitude ratio (b/a ratio). Boxes indicate the 25 and 75% quantile range, whiskers indicate the 5 and 95% quantiles and the asterisks indicate the median of the data (box-and-whisker plot). In affected $Crb2^{F/F}/Chx10Cre^{+/-}$ mice, the a-wave was relatively more attenuated than the b-wave, leading to a high b/a ratio and suggesting a predominant dysfunction of photoreceptors. (**C**) Time course of visual function based on single-flash electroretinography data from 1-, 3-, 6-, 12- and 18-month-old animals. For each age group, scotopic (SC, left column) and photopic (PH, right column) b-wave amplitude data are shown as box-and-whisker plot as above and were plotted as a function of the logarithm of the flash intensity (VlogI function). In affected $Crb2^{F/F}/Chx10Cre^{+/-}$ mice, the b-wave amplitude was already somewhat reduced at the age of 1 month under both scotopic and photopic conditions and declined rapidly with age. The retinal functionality of heterozygous $Crb2^{F/+}/Chx10Cre^{+/-}$ mice was not detectably decreased. Number of animals used: 1 month old (1 M): four/group; 3 months old (3 M): four of each control and five cKO; 6 months old (6 M): four $Crb2^{F/F}$, three $Crb2^{F/+}/Chx10Cre^{+/-}$ and seven cKO; 12 months old (12 M): five/group; 18 months old (18 M): four $Crb2^{F/F}$, three $Crb2^{F/+}/Chx10Cre^{+/-}$ and four cKO. ERG, electroretinography.

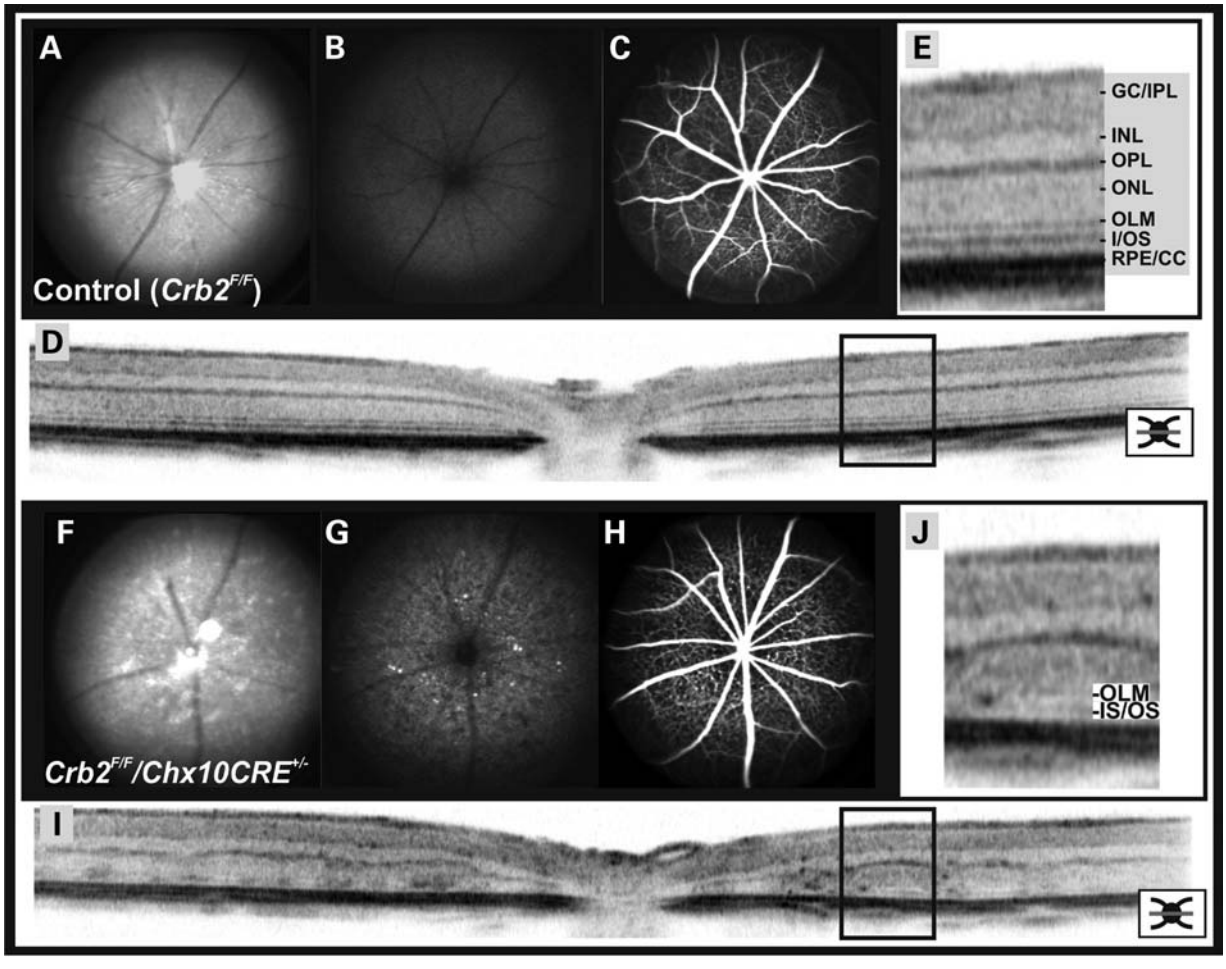

Figure 3. Retinal morphology in 1-month-old control and *Crb2*Chx10 cKO mice *in vivo*. *In vivo* imaging of the retinal phenotype in representative control (*Crb2*$^{F/F}$) and affected mice (*Crb2*$^{F/F}$/*Chx10Cre*$^{+/-}$) at 1 month after birth (1 M). Control and affected mouse retinae were examined with SLO imaging (**A** and **B** versus **F** and **G**), FLA (**C** versus **H**) and SD-OCT (**E** and **D** versus **J** and **I**). (A and F) Native fundus images at 513 nm revealed a spotty fundus appearance in the affected eye in comparison with the control, which imposed as multiple hyper- and hypofluorescences in the autofluorescence image (B and G) at 488 nm. (C and H) FLA, however, did not show apparent abnormalities of the choroidal and retinal vasculature at that point. (D and I) Horizontal spectral domain optical coherence tomography scans across the optic disc nevertheless revealed multiple indentations of the outer retina of affected eyes, presumably due to the cellular mislocalizations, disturbing retinal layering. Enlarged details (E and J) illustrate that between these indentations, intact-looking outer limiting membrane and inner/outer segment layers were detectable. GC/IPL, ganglion cell/inner plexiform layer; INL, inner nuclear layer; I/OS, inner/outer segment; OLM, outer limiting membrane; ONL, outer nuclear layer; OPL, outer plexiform layer; RPE/C, retinal pigment epithelium/choriocapillaris complex.

photoreceptors. Moreover, cone photoreceptors, stained for M-opsin (Fig. 7H and Supplementary Material, Fig. S5B–D) and cone arrestin (data not shown), were also affected and misplaced in the subretinal space. At the same stage, sporadic giant rosettes and half-rosettes in the outer nuclear layer were also observed, suggesting that there was a lack of adhesion between the cells (Supplementary Material, Fig. S4B). Transmission electron microscopy studies, performed on P10 retinas, showed disruption of the adherens junctions at the outer limiting membrane, and at these sites mislocalized photoreceptor cell nuclei were detected in the subretinal space (Fig. 9D). Furthermore, some of the cells showed polarity defects, as the segments were pointing towards the inner retina (Supplementary Material, Fig. S5C), or else were twisted (Supplementary Material, Fig. S5D) and organized in small half-rosettes around the remaining outer limiting membrane. In addition, several cone photoreceptors with abnormally long axons were detected, with axons extending from the outer plexiform layer into the ectopic nuclear layer (Supplementary Material, Fig. S5B). Ectopic PSD95 staining was detected in the photoreceptor cells misplaced in the subretinal space, suggesting the presence of ectopic synapses of these cells (data not shown). In P10 retinae, although there were no misplaced SOX9-positive cells observed in the *Crb2*Chx10 cKO (Supplementary Material, Fig. S6B), the number of Müller glia cells was 6% increased in the *Crb2*Chx10 cKO compared with the control (15.3 ± 0.2 versus 14.4 ± 0.3 SOX9-positive cells/100 μm $\pm$ SEM; Supplementary Material, Fig. S3).

Taken together, our data imply that CRB2 plays important roles in maintaining the adhesion, structural integrity, cell polarity, photoreceptor lamination, as well as controlling the differentiation of appropriate numbers of Müller glia cells and recoverin-positive cells.

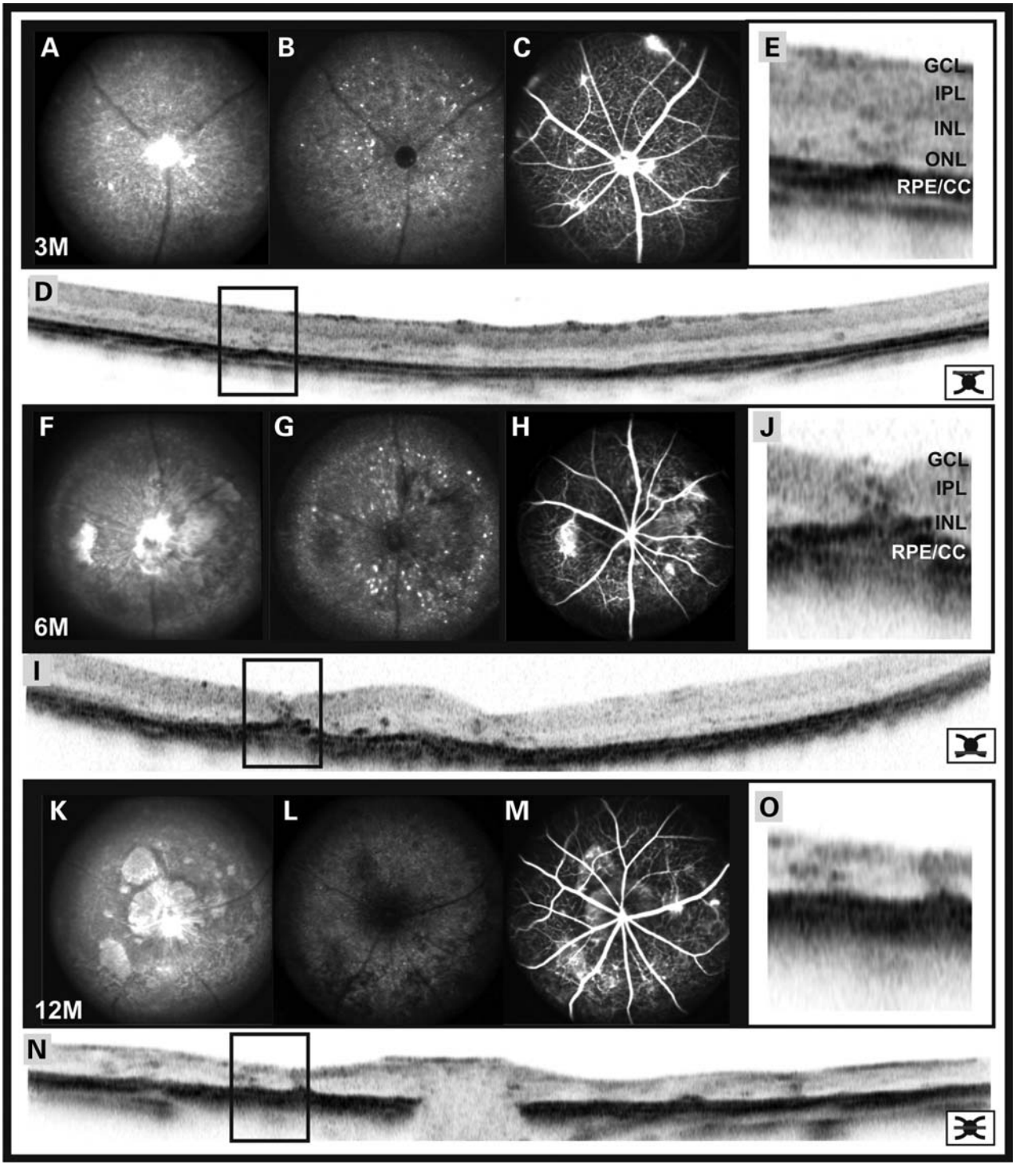

Figure 4. Progression of retinal changes in *Crb2*Chx10 cKO animals *in vivo*. Time course of retinal degeneration in representative affected mice ($Crb2^{F/F}$/$Chx10Cre^{+/-}$) up to 12 months after birth (12 M). Mouse retinae were examined with native scanning laser ophthalmoscopy imaging (**A**, **F** and **K**), fundus autofluorescence (**B**, **G** and **L**), FLA (**C**, **H** and **M**) and spectral domain optical coherence tomography (**D** and **E**, **J** and **I**, and **N** and **O**). Initially smaller, later increasingly confluent bright areas resembling retinal lesions became apparent in native imaging at 6 months (6 M) and older (F and K). Fundus autofluorescence (B, G and L) changed with age mainly in the regard that in the developing lesions described before, no fluorescence was detected, i.e. these areas remained dark. In FLA (C, H and M), sites of neovascularization developed, which were also detectable in spectral domain optical coherence tomography (D and E, J and I, and N and O). In addition, window effects led to an increased visibility of the lesion areas, particularly obvious in (M). A decrease in outer retinal thickness with disease progression was also apparent in spectral domain optical coherence tomography. GCL, ganglion cell layer; INL, inner nuclear layer; IPL, inner plexiform layer; ONL, outer nuclear layer; RPE/CC, retinal pigmented epithelium/choriocapillaris complex.

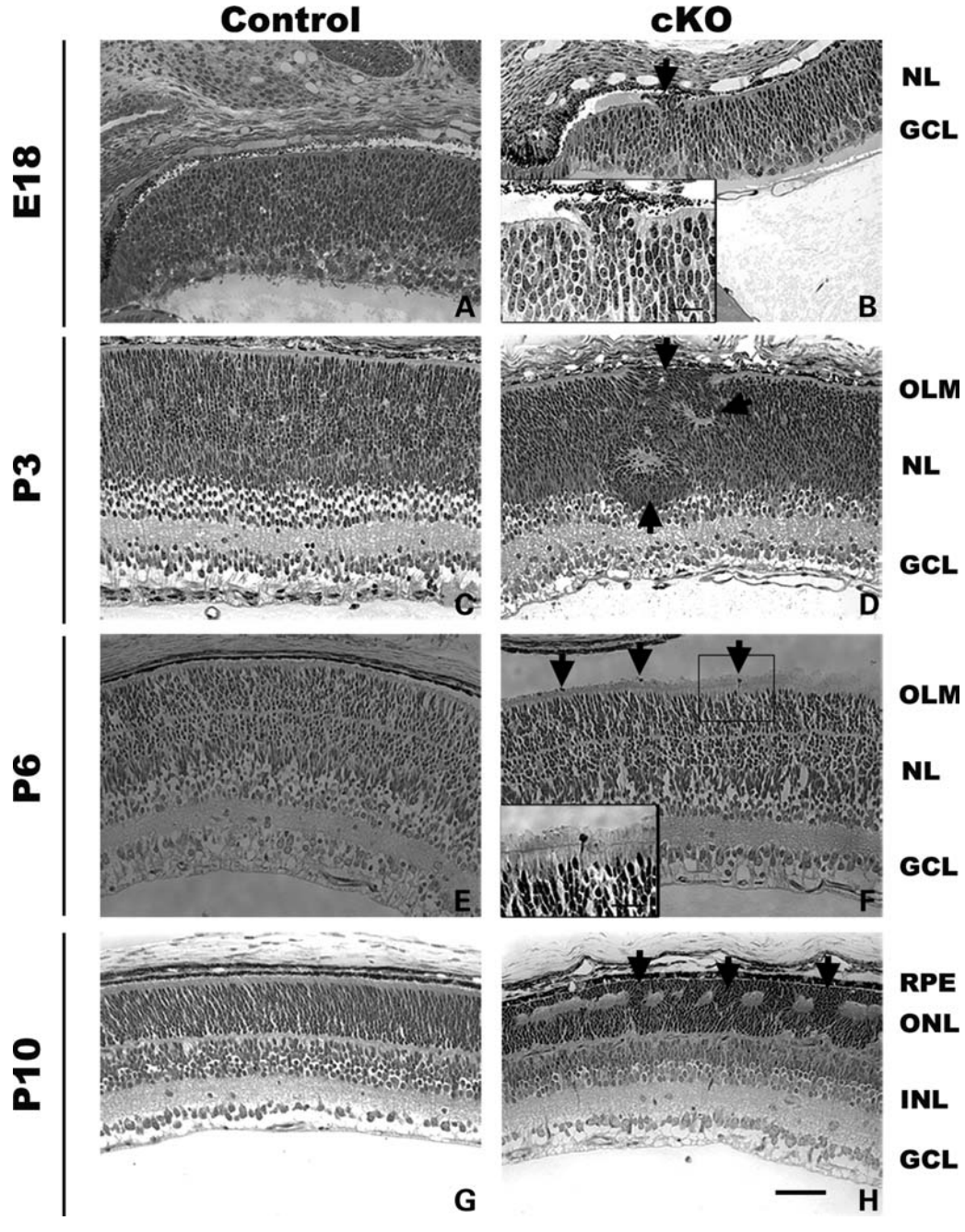

Figure 5. Loss of CRB2 results in retinal disorganization. Toluidine-stained light microscope pictures, of retina sections, from the control (**A**, **C**, **E** and **G**) and from the Crb2Chx10 cKO (**B**, **D**, **F** and **H**) at different ages: (A and B) E18; (C and D) P3; (E and F) P6; (G and H) P10. No abnormalities were observed in the control. At E18 (B) and P3 (D), gaps in the outer limiting membrane were sporadically observed in the neuroepithelial layer at the periphery. Moreover, at P3, it was also possible to detect rosettes in the neuroepithelial layer. At P6 (F), we observed some ectopic nuclei in the subretinal space. At P10 (H), a high number of nuclei were localized ectopically in the subretinal space. Disruption of the outer limiting membrane and ectopic nuclei are indicated by arrows. Scale bars: 50 μm in (A–H), and 20 μm in insets of (B) and (F). GCL, ganglion cell layer; INL, inner nuclear layer; NL, neuroepithelial layer; OLM, outer limiting membrane; ONL, outer nuclear layer; RPE, retinal pigment epithelium.

Lack of CRB2 results in progressive morphological deterioration in the adult retina

At 1 month of age, the *Crb2*Chx10 cKO retinae showed the presence of ectopic photoreceptor cell nuclei in the subretinal space and disruptions at the outer limiting membrane (Supplementary Material, Fig. S4D).

Retinal thickness gradually decreased with progressive age in the *Crb2*Chx10 cKO. This was especially apparent in the photoreceptor cell layer at the centre of the retina. At both 3

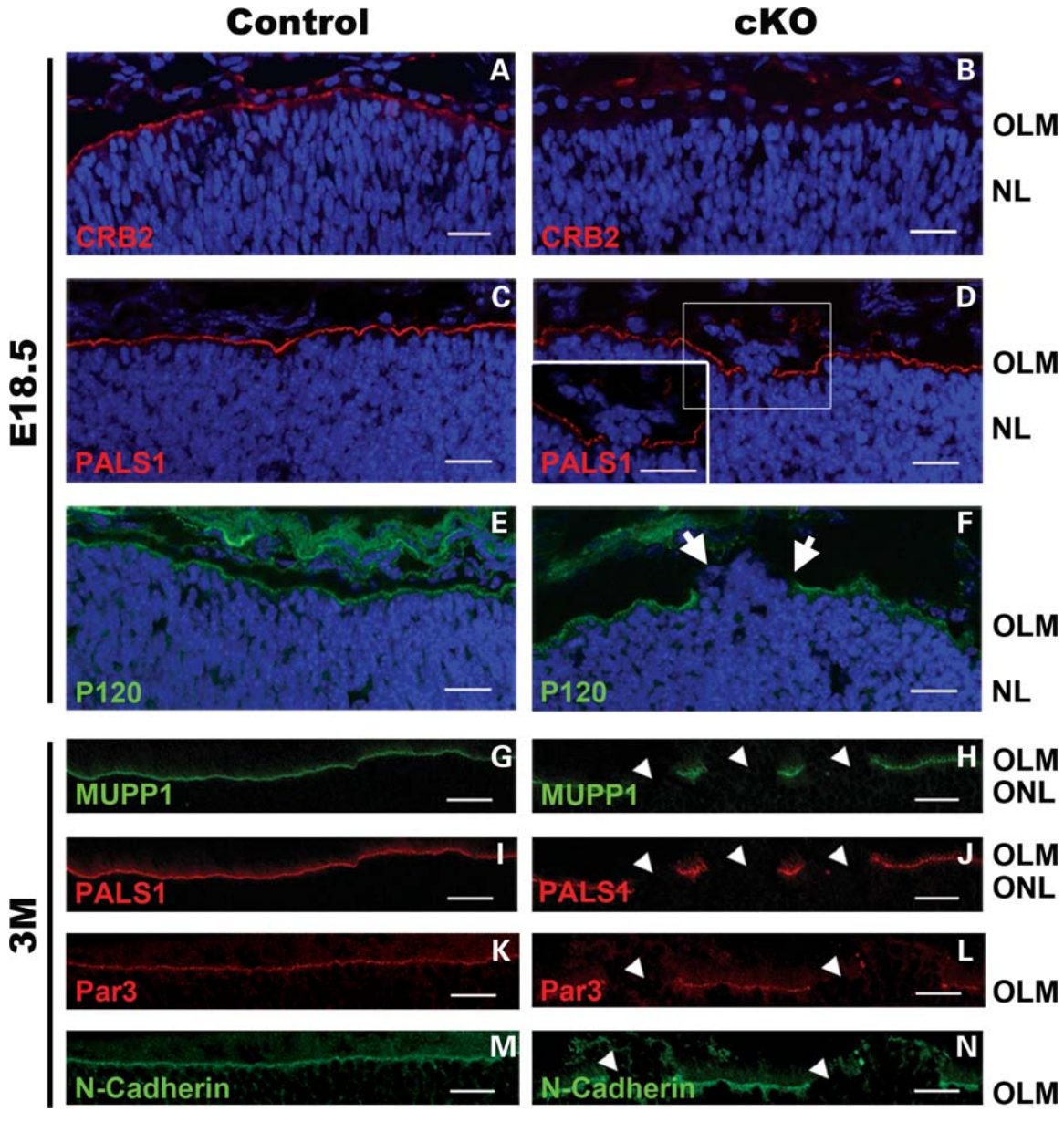

Figure 6. Lack of CRB2 leads to the disruption of the apical proteins. Immunohistochemistry pictures from the control (**A**, **C**, **E**, **G**, **I**, **K** and **M**) and from the *Crb2*Chx10 cKO (**B**, **D**, **F**, **H**, **J**, **L** and **N**) at different ages: (A–F) E18.5; (G–N) 3 months. Sections were stained with antibodies against: CRB2 (A and B), PALS1 (C, D, I and J), catenin pp120 (P120) (E and F), MUPP1 (G and H), PAR3 (K and L), N-cadherin (M and N). CRB2 was absent in the knockout retina (B), in contrast to control (A); however, it was possible to detect some signal, maybe due to cross-reactivity of the antibody with others Crumbs proteins. PALS1 and MUPP1 staining showed disruption of the Crumbs complex at the subapical region (D, H and J). PAR3 was also lost at sites of disruption (L). Staining using adherens junctions markers P120 (F) and N-cadherin (N) showed disruption of the adherens junctions. Moreover, it was also possible to visualize ectopic nuclei protruding into the subretinal space (arrows). No morphological changes were observed in the control retinae. NL, neuroepithelial layer; OLM, outer limiting membrane; ONL, outer nuclear layer. Scale bars: 20 μm.

and 6 months of age, we observed regions with several rows of photoreceptor cell nuclei protruding into the subretinal space, gaps in the outer limiting membrane and similarly protrusions of inner nuclear layer cells into the outer nuclear layer (Supplementary Material, Fig. S4F and H). We examined 3-month-old retinae in detail using immunohistochemistry. In control retinae, the Crumbs complex members MUPP1 and PALS1 (Fig. 6G and I) and CRB1 and PATJ (data not shown) stained the subapical region adjacent to the outer limiting membrane. In contrast, in *Crb2*Chx10 cKO retinae, the staining for subapical region proteins was absent in the regions with protrusions of photoreceptor nuclei into the subretinal space (Fig. 6H and J). Staining for markers of the adherens junctions at the outer limiting membrane (cadherins, β-catenin, catenin p120) and PAR3 gave similar results (Fig. 6L and N). The recoverin and rhodopsin staining indicated a clear decrease in the thickness of the *Crb2*Chx10 cKO outer nuclear layer and photoreceptor segments (Fig. 7J). Furthermore, the cone photoreceptor morphology was highly affected, with the loss of segments and incorrect

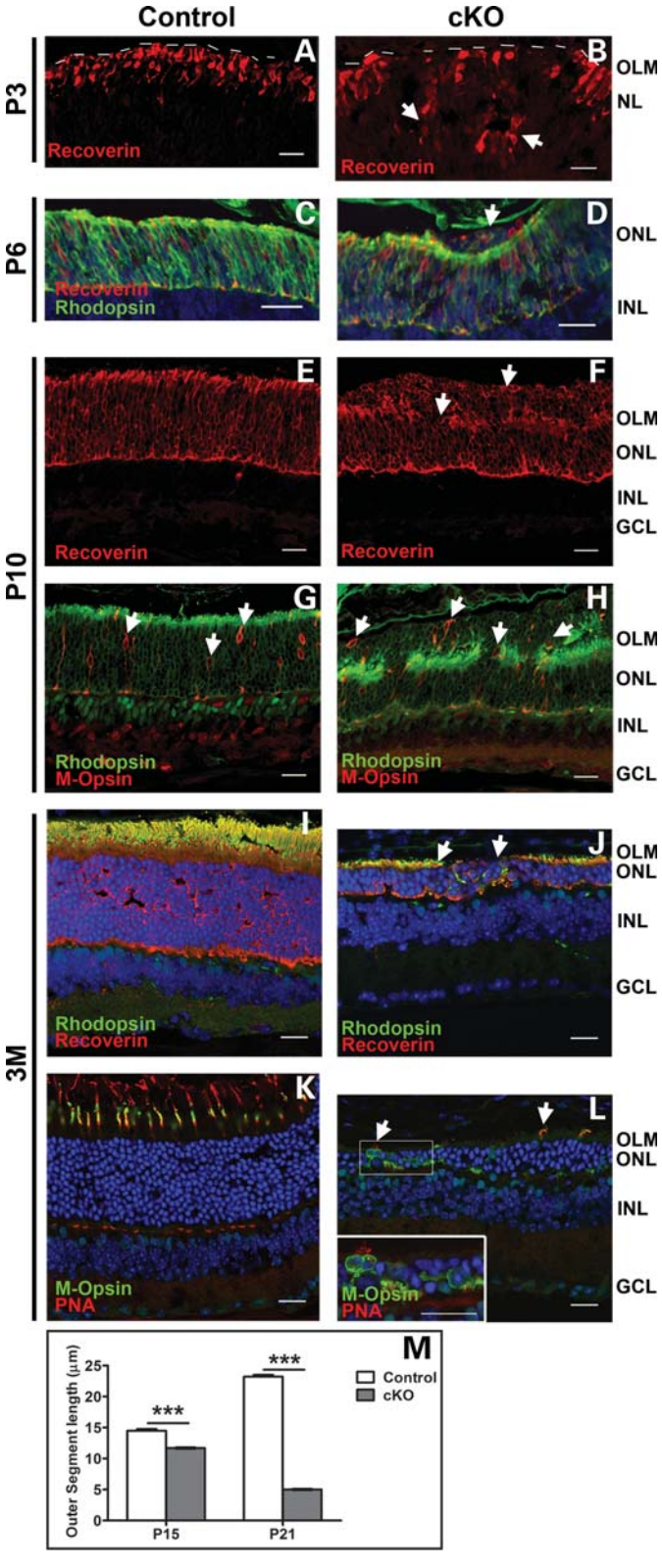

Figure 7. Loss of CRB2 affects lamination of photoreceptor cells and photoreceptor outer segment length. Immunohistochemistry pictures from mouse retinae with ages comprehended between P3 and 3 months (3 M). Retina sections of the control (**A**, **C**, **E**, **G**, **I** and **K**) and of the *Crb2*Chx10 cKO (**B**, **D**, **F**, **H**, **J** and **L**) at the different time points: (A and B) P3; (C and D) P6; (E, F, G and H) P10; (I, J, K and L) 3 months. Sections were stained with antibodies against: recoverin (A and B, E and F), recoverin and rhodopsin (C and D, I and J), rhodopsin and M-opsin (G and H), M-opsin and peanut agglutinin (K and L). At P3 and P6, the knockout retinae presented disorganization of the photoreceptor cells, stained with recoverin (B and D). Close to the periphery, we could detect photoreceptors, rosettes and half-rosettes in the neuroepithelial layer (B, arrows). Ectopic nuclei could be found in the subretinal space at P6. Some of these cells were recoverin-positive but rhodopsin-negative, a mature rod photoreceptor marker (D, arrow). At P10, most of the nuclei localized in the subretinal space were positive for recoverin (F) and rhodopsin (H). However, some of these nuclei were M-opsin-positive, showing that also cone photoreceptors were misplaced (H, arrows). At 3 months of age, the photoreceptor layer of the *Crb2*Chx10 cKO retinae was reduced to few nuclei in a row when stained with recoverin (J). Rhodopsin is normally localized in the outer segments of the photoreceptors (I), but in the knockout retinae besides the reduced length of the segments, it is possible to detect some ectopic cytoplasmic localization of this protein (J). In the control, anti-M-opsin and peanut agglutinin stain mainly the segments of the photoreceptors (K); however, in the knockout retinae, the cones are heavily affected, especially their segments, with ectopic localization of the M-opsins in the cell bodies (L, inset). No morphological changes were observed in the control retinae. (M) Histogram showing the length of cone outer segments in the retinae from littermate control (white bars) and *Crb2*Chx10 cKO (grey bars) retinae at P15 and P21. The peanut agglutinin-stained cone outer segments in the central region were measured to verify the involvement of CRB2 in the growth and maintenance of cone outer segments; significant differences were found at P15 (control = 3 mice, $n = 320$; cKO = 3 mice, $n = 352$) and P21 (control = 3 mice, $n = 606$; cKO = 3 mice, $n = 472$). Asterisks indicate a significant difference compared with the control (Student's *t*-test). Error bars indicate $\pm$SEM. INL, inner nuclear layer; GCL, ganglion cell layer; NL, neuroepithelial layer; OLM, outer limiting membrane; ONL, outer nuclear layer. Scale bars: 20 μm.

expression of S- and M-opsins in the cell soma (Fig. 7L and Supplementary Material, Fig. S5H). Despite this severe phenotype, the cone photoreceptors survived in *Crb2*Chx10 cKO retinae, even in areas where only few photoreceptor nuclei remained.

Throughout the 3-month-old *Crb2*Chx10 cKO retina, we observed an increase in GFAP expression (a marker of intermediate filaments in Müller glia cells; Fig. 10D and F). Abnormal expression of SOX9 and glutamine synthetase in the mutant outer nuclear layer indicated the presence of ectopic Müller glia cell nuclei in this region (Fig. 10H). These cells were negative for the proliferation marker pH3 (data not shown). Interestingly, at this age, we also observed an increase of 12% in the total number of SOX9-positive cells in the *Crb2*Chx10 cKO compared with the control (17.6 ± 0.5 versus 15.5 ± 0.5 SOX9-positive cells/100 μm $\pm$ SEM; Supplementary Material, Fig. S3).

In *Crb2*Chx10 cKO retina, we observed a marked increase in CD45 and CD11b expression, two microglia cell markers (Supplementary Material, Fig. S6D and F). This expression extended into the outer retinal layers. MPP4 is present at the synapses of photoreceptors, and at lower levels at the outer limiting membrane; in control retinae, it is expressed in a continuous band at the outer limiting membrane and outer plexiform layer (Supplementary Material, Fig. S6G) (15). In the *Crb2*Chx10 cKO retinae, the outer plexiform layer was thinner and MPP4 staining was disrupted (Supplementary Material, Fig. S6H). The synapses of the photoreceptor cone cells appeared less well defined when stained with peanut agglutinin (Fig. 7L and Supplementary Material, Fig. S5H) and anti-cone arrestin (Supplementary Material, Fig. S5F).

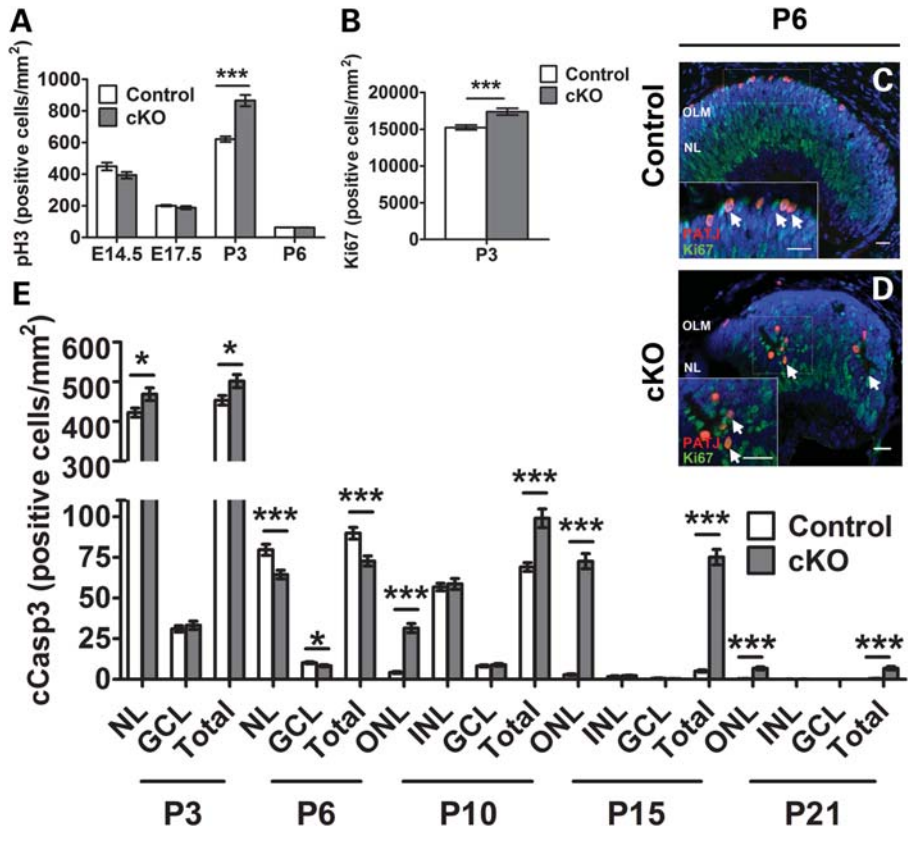

Figure 8. Loss of CRB2 affects timing of apoptosis and mitosis. (**A**) Histogram depicting the number of pH3-positive cells per square millimetre, in control and *Crb2*Chx10 cKO retinae, at E14.5 (control = 3 mice, cKO = 4 mice; $n = 31$ and $n = 26$, respectively), E17.5 (4 mice/group; $n = 118$ and $n = 93$, respectively), P3 (control = 4 mice, cKO = 3 mice; $n = 118$ and $n = 92$, respectively) and P6 (control = 3 mice, cKO = 4 mice; $n = 97$ and $n = 100$, respectively). Error bars indicate $\pm$SEM. (**B**) Histogram depicting the number of Ki67-positive cells per square millimetre, in control and *Crb2*Chx10 cKO retinae, at P3 (3 mice/group; $n = 29$ and $n = 29$, respectively). Error bars indicate $\pm$SEM. (**C** and **D**) Immunohistochemistry pictures from P6 mouse retinae. Retina sections of the control (C) and of the *Crb2*Chx10 cKO (D) were stained with antibodies against Ki67 and PATJ (C and D). In the knockout retina (D), misplaced Ki67-positive mitotic cells were detected. The apical marker PATJ co-stains a subset of Ki67-positive cells at the periphery of the developing retina. Scale bars: 20 μm. (**E**) Histogram depicting the number of cCasp3-positive cells, a marker for apoptosis, per square millimetre, in control and *Crb2*Chx10 cKO retinae at P3 (3 mice/group; $n = 31$ and $n = 26$, respectively), P6 (control = 3 mice, cKO = 4 mice; $n = 75$ and $n = 87$, respectively), P10 (3 mice/group; $n = 80$ and $n = 70$, respectively), P15 (3 mice/group; $n = 30$ and $n = 45$, respectively) and P21 (control = 3 mice, cKO = 4 mice; $n = 62$ and $n = 45$, respectively). Asterisks indicate a significant difference compared with the control. Student's *t*-test for P3, Mann–Whitney *U* test for P6, P10, P15 and P21. Error bars indicate $\pm$SEM. GCL, ganglion cell layer; INL, inner nuclear layer; NL, neuroepithelial layer; OLM, outer limiting membrane; ONL, outer nuclear layer.

The morphology and location of the bipolar cells were also affected in the *Crb2*Chx10 cKO. In adult Chx10-*Cre* retinae, the Cre protein is fused with EGFP and can be detected in the nuclei of some bipolar cells (28). Using this, we could observe misplaced *Crb2*Chx10 cKO bipolar cell nuclei in the outer nuclear layer. At 3 months of age, PKCα expression indicated that these cells showed fewer dendrites (Supplementary Material, Fig. S6H). Nevertheless, in some areas in the *Crb2*Chx10 cKO retinae, we observed long dendritic projections almost up to the outer limiting membrane (data not shown). The tip of the ectopic dendrites colocalized with MPP4 expression, suggesting ectopic photoreceptor-bipolar cell synapses (data not shown). Other inner retinal cells, such as calretinin-positive amacrine cells, showed normal localization at 3 months of age (Supplementary Material, Fig. S6J).

In contrast to earlier time points, by 12 and 18 months of age the entire *Crb2*Chx10 cKO retina was affected (Supplementary Material, Fig. S4J and L). Very few photoreceptor cells remained. Large and numerous retinal blood vessels were detected. The retinal pigment epithelium was also affected; in some areas, the epithelium was disrupted and protruded into the retina.

Loss of CRB2 affects progenitor proliferation, rod photoreceptor apoptosis and cone photoreceptor outer segment size

To study whether CRB2 plays a role in determining the length of photoreceptor outer segments, we quantified the length of cone photoreceptor outer segments, marked with peanut agglutinin (a marker for the outer segments and pedicles of cone photoreceptors). In *Crb2*Chx10 cKO retinae, we observed shorter cone outer segments at P15 (11.7 ± 0.3 μm compared with the control 14.5 ± 0.2 μm $\pm$ SEM) and P21 (5 ± 0.2 μm compared with the control 23.2 ± 0.3 μm $\pm$ SEM) (Fig. 7M), suggesting that CRB2 may play a role in determining the length of cone photoreceptor outer segments.

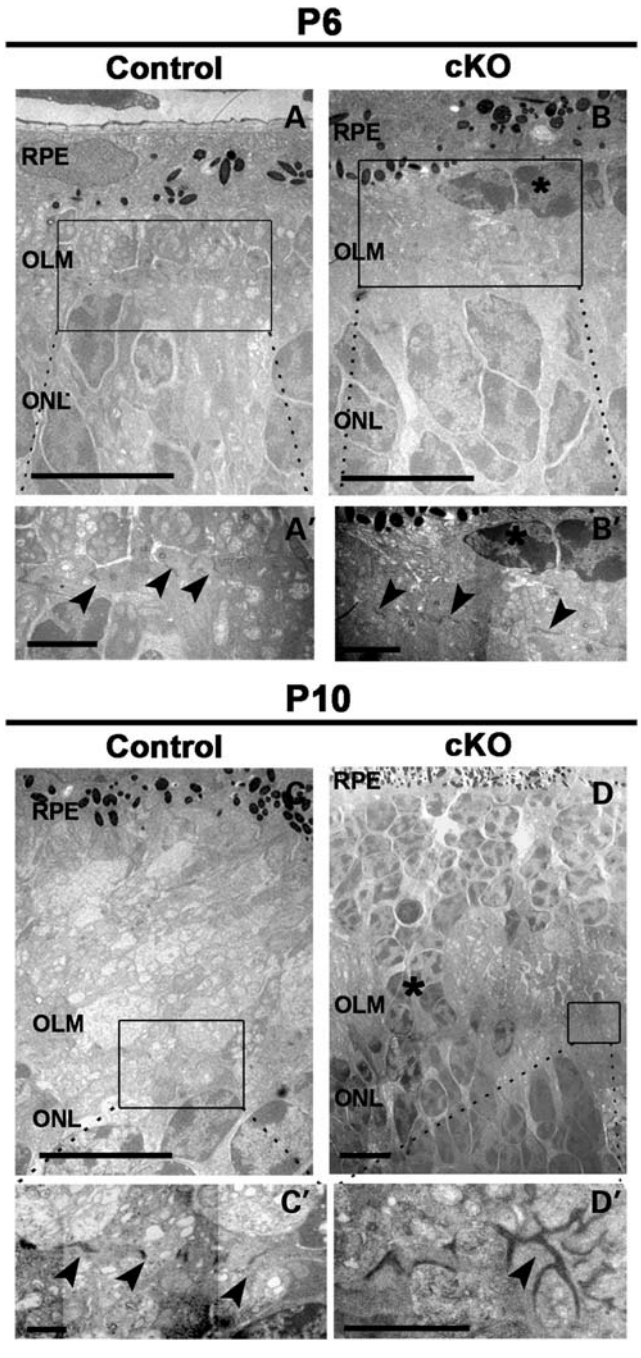

Figure 9. Loss of CRB2 results in the disruption of the adherens junctions. Transmission electron microscopy pictures of retinae sections, from the control (**A** and **C**) and from the *Crb2*Chx10 cKO (**B** and **D**), at different ages: (A and B) P6; (C and D) P10. No abnormalities were observed in the control. At P6 in the *Crb2*Chx10 cKO retinas, ectopic nuclei (asterisk) located in the subretinal space were observed (B). Disruption in the adherens junctions were observed at the level of the ectopic nuclei (**B′**). At P10, a high number of nuclei were localized ectopically in the subretinal space (D, asterisk), and clusters of the adherens junctions were also observed (**D′**). Scale bars in (A–D): 7.5 μm, and in (**A′**–**D′**): 2.5 μm. OLM, outer limiting membrane; ONL, outer nuclear layer; RPE, retinal pigment epithelium.

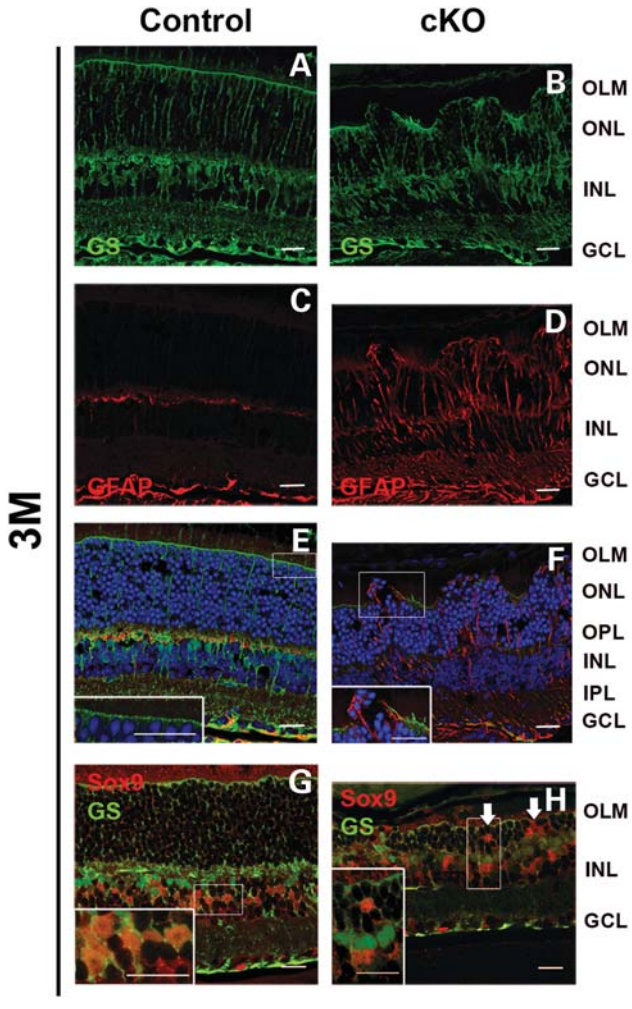

Figure 10. Lack of CRB2 results in retinal gliosis. Immunohistochemistry pictures of 3-month-old retina sections. Sections from the control (**A**, **C**, **E** and **F**) and from the *Crb2*Chx10 cKO (**B**, **D**, F and **H**) were stained with antibodies against: glutamine synthetase (GS) (A and B), glial fibrillary acidic protein (GFAP) (C and D), GS and GFAP (merged) (E and F), GS and SOX9 (**G** and H). The *Crb2*Chx10 cKO retinae showed activated Müller glia cells, detected by an increase in the GFAP staining (D and F). Some nuclei of the Müller glia cells were mislocalized in the outer nuclear layer (H). GCL, ganglion cell layer; INL, inner nuclear layer; IPL, inner plexiform layer; OLM, outer limiting membrane; ONL, outer nuclear layer; OPL, outer plexiform layer. Scale bars: 20 μm.

The number of pH3- and Ki67-positive cells was significantly increased at P3 in the *Crb2*Chx10 cKO retinae compared with the controls (Fig. 8A and B). However, no difference in the number of pH3-positive cells was detected at E14.5, E17.5 or P6, implying that the presence of CRB2 is required to control the proliferation of late-born progenitor cells around the peak of birth of Müller glia cells, rods and bipolar cells.

Programmed cell death, detected by the number of cleaved caspase-3 (cCasp3)-positive cells, was significantly higher in *Crb2*Chx10 cKO retinae at P3, P10, P15 and P21 but not at P6, where a decrease in apoptosis is observed (Fig. 8E). The decrease in apoptosis, at P6, may reflect a shift in the apoptosis timing or an increase in cell survival at this time point. Interestingly, increased apoptosis affected only cells in the photoreceptor layer and not in the inner nuclear layer or ganglion cell layer. In the mutant retina, the peak in the number of

apoptotic cells occurred around P15, where a 10-fold increase of apoptotic cells was observed. At P10 and P15, the number of apoptotic rod photoreceptors was equally divided between ectopic and correctly localized cells.

DISCUSSION

Our key findings are that retinal CRB2 is required for: (i) correct expression and/or localization of apical complex and adherens junction proteins, (ii) proper lamination of photoreceptor cells, and (iii) suppression of birth of late-born progenitor cells. Moreover, in addition to these late developmental defects, the adult *Crb2*Chx10 cKO retina undergoes progressive rod photoreceptor degeneration with associated loss of retinal function that mimics retinitis pigmentosa due to mutations in the *CRB1* gene.

We have shown that CRB2 colocalizes with other apical marker proteins in the retina. Depletion of CRB2 resulted in the loss of other apical and some adherens junction protein markers, suggesting that reduction in CRB2 levels leads to the destabilization of the whole CRB complex and its interacting complexes. Our observation is therefore consistent with the epithelial polarity and adhesion defects seen in both the *Drosophila Crb* mutant and the zebrafish *Crb2a* (*ome*) mutant (9,11,21). However, in the *Crb2*Chx10 cKO retina, the phenotype did affect the late but not the early retinal neuroepithelium despite the fact that CRB2 has been lost throughout. Our results are also partially in consonance with the phenotype detected in mice with reduced retinal levels of PALS1, a CRB interacting protein, as both show retinal degeneration affecting lamination of the photoreceptor layer (4,6). In the retinal neuroepithelium, the absence of CRB2 results in inappropriate numbers of Müller glia cells and rod photoreceptor cells, with many of the latter appearing to remain with an immature expression profile for longer than in controls. Interestingly, these retinal cell types are the ones born last from a retinal precursor that experiences a changing micro-environment (31). We found that there was a significant increase in pH3- and Ki67-positive cells at P3. This would correlate approximately with the time when the cells may be undergoing their last symmetric post-mitotic cell division (32). This suggests that CRB2 inhibits retinal progenitor proliferation in the late developing retina.

In the developing retina, we found that the loss of CRB2 during retinal development results in ectopic Ki67/PATJ-positive cells and displaced recoverin-positive photoreceptor cells. Ectopic *Crb2*Chx10 cKO bipolar cell and Müller glia cell nuclei were also apparent in the outer nuclear layer at 3 months of age. The lamination of earlier born progenitor, ganglion, horizontal, amacrine cells and Müller glia cells was not affected. Furthermore, the lamination defects seem to affect mainly late-born retinal progenitors, rod and, to some extent, cone photoreceptors and bipolar cells, suggesting a lack of adhesion between these cells. This is consistent with data that show a role for zebrafish Crb2a in retinal cell patterning and lamination (26). Moreover, reduced levels of PALS1, in mouse retinae, affected the correct patterning of newly born retinal cells, especially photoreceptors (4,6).

Zebrafish Crb2 interacts directly with the extracellular domain of Notch and inhibits its activity. Further data suggest that the zebrafish CRB–Moe complex and Notch play key roles in a positive feedback loop to maintain apicobasal polarity and the apical-high–basal-low gradient of Notch activity in neuroepithelial cells (33). For mammals, this will be further explored in forthcoming experiments.

It has been suggested that Crumbs proteins play a role in determining the length of the photoreceptor cell segments. Our data show that the loss of CRB2 results in shorter cone photoreceptor outer segments, consistent with the roles of zebrafish Crb2b in cone photoreceptors (11), of *Drosophila* Crb in determining the length of the stalk membrane, which is the functional equivalent of vertebrate inner segments (9) and of mouse CRB1 in determining the length of the apical villi of Müller glia cells (3).

The retinae of Leber congenital amaurosis patients with *CRB1* mutations are relatively thick and resemble the immature retina, suggesting a disturbance in normal development (34,35). To date, no mutations in *CRB2* or *CRB3* have been associated with retinal degeneration. However, it cannot be excluded that some sequence variants may contribute to retinal disease (36). Our previous results showed that $Crb1^{-/-}$ mouse retinae develop localized lesions, particularly in the inferior temporal quadrant of the mouse eye, after retinal development (3). *Crb2*Chx10 cKO mice developed early disorganization and degeneration throughout the entire retina during late retinal development, suggesting that CRB2 is required for proper lamination of the entire photoreceptor layer. Mice lacking functional CRB1 do not become blind, and since there may be functional redundancy between CRB family members (1–3,8,11,35), *Crb2* and *Crb1Crb2* double-cKO mice may become valuable in functionally testing *CRB1* gene therapy vectors *in vivo*.

MATERIALS AND METHODS

Animals

All procedures concerning animals were performed with the permission of the animal experimentation committee (DEC) of the Royal Netherlands Academy of Arts and Sciences (KNAW) (permit number NIN06–46). All mice used were maintained on a 50% C57BL/6JOlaHsd and 50% 129/Ola genetic background. Animals were maintained on a 12 h day/night cycle and supplied with food and water *ad libitum*.

Generation of the *Crb2* cKO mouse

Using recombineering in bacterial artificial chromosomes (BACs) and *Cre/loxP* technology (37), we generated a conditional gene targeting construct for *Crb2*. Details are available upon request. In short, a 3′ *loxP* site was inserted in exon 13 downstream the stop codon in the 3′ untranslated region of *Crb2*. A neomycin cassette flanked by *frt* recombination sites and a 5′ *loxP* site was inserted in intron 9 downstream exon 9a. The targeting vector was released from the BAC into a plasmid using homologous recombineering. The *Crb2* gene is expressed from two different promoters that are far apart (unpublished data); therefore, the *Crb2* targeting vector

has been designed to put *loxP* recombination sites around the last four coding exons (10–13) of the gene that encode the CRB2 transmembrane domain and the 37 amino acids of the C-terminal intracellular domain. Cre-mediated recombination deleted coding exons 10–13 and resulted in a nonsense mutation with premature truncation of CRB2 protein at amino acid 871. The Cre recombination therefore removed both the transmembrane domain and the highly conserved 37 amino acids intracellular domain that contains the functionally significant FERM and PDZ protein-binding motifs. The function of the *loxP* and *frt* recombination sites was tested by expression of the floxed *Crb2* targeting vector in bacterial cells expressing CRE or FLP recombinases. The targeting vector was used to generate $Crb2^{F/+}$ mouse 129 E14 embryonic stem cells by homologous recombination. The $Crb2^{F/+}$ cKO mice were generated by blastocyst injections of $Crb2^{F/+}$ embryonic stem cells. Chimeric mice gave germ-line transmission, then the neomycin cassette was successfully removed by crossing the $Crb2^{F/+}$ mice with a transgenic mouse that expressed FLP recombinase in the germ line (129S4/SvJaeSort(ROSA)26Sortm1(*FLP1*)Dym/J mice; Jackson Laboratory). Two $Crb2^{F/+}$ mouse lines were generated from two independent embryonic stem cell clones; these lines were designated P1E9 and P11D6. The two lines gave identical phenotypes.

Genotyping was performed by Southern blotting, long-distance PCR and PCR. For Southern blotting, *Bgl*II-digested genomic DNA was transferred to Hybond N+ membrane (GE Healthcare, Germany), UV-crosslinked and hybridized to radiolabelled probes. PCR genotyping of mice was performed using primers flanking the *loxP* sites. The cKO mice were crossed with Chx10-*Cre* (Jackson Laboratory) expressing CRE recombinase in the developing neuroepithelium of the retina (28).

Chromosomal DNA isolation and genotyping

Ear biopsies were incubated in lysis buffer (50 mM Tris, pH 8.0, 100 mM NaCl, 1% SDS) with Proteinase K (0.5 mg/ml) at 55°C for 16 h. The isopropanol precipitated chromosomal DNA was washed with 80% ethanol and rehydrated in TE buffer. The localization of the primers used to genotype the targeting construct is represented in Figure 1. Two different pair of primers were used to genotype the transgenic floxed offspring via PCR using genomic DNA extracted from biopsies: HA7 forward 5′-TGCATCTTCTGAGATCAGGTG-3′, HA8 reverse 5′-ACCTGCCAGACTTCTCCTAC-3′ (*Δfrt*) [*Δfrt*: 303 base pairs (bp)/wild-type (WT): 106 bp], HA11 forward 5′-TGGAGATGGACAGTGTCCTC-3′, HA12 reverse 5′-GCTCTGGAAACAGTCTCCTTG-3′ (*LoxP*) (Flox: 217 bp/WT: 185 bp). To analyse the presence of the *flp* recombinase, the following primers were used: FLP (transgenic) forward 5′-CACTGATATTGTAAGTAGTTTGC-3′, reverse 5′-CTA GTGCGAAGTAGTGATCAGG-3′ (product size 725 bp), FLP (WT) forward 5′-GGAAAATGCCAATGCTCTGT-3′, reverse 5′-ACGTTTCCGACTTGAGTTGC-3′ (product size 835 bp). The presence of the neomycin cassette was analysed using the following primers: forward 5′-CGGACAGGTC GGTCTTGACA-3′ and reverse 5′-TGAGCCTGGCGAACA GTTCG-3′ (product size 380 bp). The following primers were used to detect the transgenic *Cre* expression: Chx10-*Cre* forward 5′-GGGCACCTGGGACCAACTTCACGA-3′, reverse 5′-CGGCGGCGGTCACGAACTCC-3′ (product size 750 bp).

In vivo analysis

Scanning laser ophthalmoscopy, spectral domain optical coherence tomography and electroretinography measurements were performed in animals groups of 1, 3, 6, 12 and 18 month(s). The groups were composed of four to six animals of each genotype: controls ($Crb2^{F/F}$ and $Crb2^{F/+}/Chx10Cre^{+/-}$) and *Crb2*Chx10 cKO ($Crb2^{F/F}/Chx10Cre^{+/-}$).

Electroretinographic analysis

Electroretinograms were performed according to previously described procedures (38). The electroretinography equipment consisted of a Ganzfeld bowl, a direct current amplifier and a PC-based control and recording unit (Multiliner Vision). Animals were dark-adapted overnight and anaesthetized with ketamine (66.7 mg/kg body weight) and xylazine (11.7 mg/kg body weight). Pupils were dilated with tropicamide eye drops (Mydriaticum Stulln, Pharma Stulln, Stulln, Germany). Single-flash responses were obtained under dark-adapted (scotopic) and light-adapted (photopic) conditions. Light adaptation was accomplished with a background illumination of 30 candela (cd) per square metre, starting 10 min before photopic recordings. Single white-flash stimuli ranged from −4 to 1.5 log cd s/m^2 under scotopic and from −2 to 1.5 log cd s/m^2 under photopic conditions. Ten responses were averaged with inter-stimulus intervals of 5 s (for −4 to −0.5 log cd s/m^2) or 17 s (for 0–1.5 log cd s/m^2).

Scanning laser ophthalmoscopy and angiography

Retinal structures of the anaesthetized animals were visualized via scanning laser ophthalmoscopy imaging with HRA 1 and HRA 2 (Heidelberg Engineering, Heidelberg, Germany), according to previously described procedures (39). Briefly, HRA 1 and HRA 2 systems feature two lasers (488/514 nm) in the short (visible) wavelength range and two (795/830 nm and 785/815 nm) in the long (infrared) wavelength range. The 488 and 795 nm lasers are used for FLA and indocyanine green angiography, respectively.

Spectral domain optical coherence tomography

Spectral domain optical coherence tomography imaging was done in the same session as scanning laser ophthalmoscopy and it was performed with a commercially available Spectralis^{TM} HRA + OCT device from Heidelberg Engineering, featuring a broadband superluminescent diode at $\lambda =$ 870 nm as a low-coherent light source (40). Each two-dimensional B-Scan recorded with the equipment set to 30° field of view consists of 1536 A-scans acquired at a speed of 40 000 scans per second. Optical depth resolution is ∼7 μm, with digital resolution reaching 3.5 μm. Imaging was performed using the proprietary software package Eye Explorer (version 3.2.1.0, Heidelberg Engineering).

Morphological and immunohistochemical analyses

Eyes were collected at different time points: E11.5, E12.5, E14.5, E16.5, E17.5, E18.5; P3, P6, P10, P15, P21; 1-, 3-, 6-, 12- and 18-month-old mice ($n = 3–6$/age group). For morphological analysis, eyes were enucleated and fixed at room temperature with 4% paraformaldehyde in PBS for 20 min. After fixation, the eyes were dehydrated for 30 min in 30, 50, 70, 90 and 96% ethanol and embedded in Technovit 7100 (Kulzer, Wehrheim, Germany), according to the manufacturer's instructions and sectioned (3 μm). Slides were dried, counterstained with 0.5% toluidine blue and mounted under cover slips, using Entellan (Merk, Darmstadt, Germany). For immunohistochemical analysis, eyes from the animals were enucleated and fixed during 20 min in 4% paraformaldehyde in PBS. Subsequently, the tissues were cryoprotected with 30% sucrose in PBS, embedded in Tissue-Tek O.C.T. Compound (Sakura, Finetek) and used for cryosectioning. Cryosections (7 μm) were rehydrated in PBS. For Ki67 stainings, heat-mediated antigen retrieval was performed before the blocking step, sections were boiled at 95–100°C for 2 min in 10 mM sodium citrate buffer with 0.05% Tween-20, pH 6.0, and allowed to cool down for 30 min. Samples were blocked for 1 h using 10% goat or donkey serum, 0.4% Triton X-100 and 1% bovine serum albumin (BSA) in PBS. The following primary antibodies were used: β-catenin (1:100; BD Biosciences), catenin pp120 (P120) (1:100; BD Biosciences), N-cadherin (1:100, BD Biosciences), calretinin (1:500, Chemicon), APC-conjugated CD11b (1:100; eBioscience), PE-conjugated CD45 (1:100; Emeelca), cCasp3 (1:250; Cell Signaling), cone arrestin (1:500, Millipore), CRB1 (AK2, 1:100), CRB2 (SK11; 1:700, obtained from P.R.), glial fibrilliary acidic protein (GFAP) (1:200; Dako), glutamine synthetase (1:200; BD Biosciences), Ki67 (1:50, BD Biosciences), M-opsin (1:250; Chemicon), S-opsin (1:250; Chemicon), PALS1 (1:1000; Proteintech), PAR3 (1:100, Upstate), PATJ (1:250, obtained from A.L.B.), PAX6 (1:100; Developmental Studies Hybridoma Bank), rhodamine peanut agglutinin (1:150; Vector Lab), pH3 (1:500; Millipore), PKCα (1:200; BD Biosciences), PSD-95 (1:200, Cell Signaling), recoverin (1:500; Chemicon), rhodopsin (1:250; Millipore), MPP4 (AK4, 1:300), MUPP1 (1:200; BD Biosciences), SOX9 (1:250, Millipore). The primary antibodies were diluted in 0.3% goat or donkey serum, 0.4% Triton X-100 and 1% BSA in PBS and incubated for 16 h at 4°C. Fluorescent-labelled secondary antibodies, donkey anti-chicken, goat anti-mouse or goat anti-rabbit IgGs conjugated to Cy3, Alexa 488 or Alexa 555 (1:500; Jackson ImmunoResearch, Stanford, CA, USA, and Invitrogen), were diluted in 0.1% goat or donkey serum in PBS and incubated for 1 h at room temperature. Nuclei were counterstained using the DNA dye TO-PRO-3 iodine (Invitrogen) at 1 μM. Sections were mounted under cover slips using Mowiol 4–88 (Sigma-Aldrich) to prevent fading of fluorescence. Sections were imaged on a Zeiss 510 confocal laser scanning microscope (CLSM) or on a Leica SP5 CLSM. Confocal images were processed with Adobe Photoshop CS4 extended v11.0.1.

Transmission electron microscopy

Mice of 6 and 10 days of age were perfused with 4% paraformaldehyde, 2% glutaraldehyde in 0.1 M cacodylate buffer, pH 7.4. The eyes were opened along the ora serrata. The cornea, lens and vitreous body were removed. After the retinae were dissected free, they were post-fixed for 1 h in 1% osmium tetroxide in the same buffer. Tissues were abundantly rinsed with the buffer and stained with 2% uranyl acetate in 70% ethanol for 1 h. Samples were then dehydrated in a graded series of ethanol and embedded in Epon 812 (Polysciences, Eppelheim, Germany). Ultrathin sections were examined with a Zeiss 912 electron microscope (Zeiss).

Quantification of apoptotic, mitotic and retina cells

Retina sections (P3, P6, P10, P15 and P21) were stained with cCasp3 antibody to quantify the number of apoptotic cells. To quantify the number of mitotic cells, retina sections (E14.5, E17.5, P3 and P6) were stained with pH3 antibody. The number of proliferating cells at P3 was quantified using Ki67 staining. To study defects in late-born cell specification, the number of photoreceptor cells, Müller glia cells and bipolar cells was quantified at different time points using specific antibodies. To count photoreceptor cells, a recoverin antibody was used at P3. Müller glia cells were counted at P10 and 3 M using a SOX9 antibody. Bipolar cells were counted at 3 M using a PKCα antibody. Ten to 20 retina sections from three to six different *Crb2*Chx10 cKO and control mice were used. Retina sections were counterstained and mounted with Vectashield Hard-Set Mounting Medium with DAPI (H1500, Vector Laboratories). The total number of cells was determined by manually counting the positive cells, and digital images were generated by a Leica epifluorescence microscope (DMRD), using the LAS AF v2.4.1 software (n represents the number of individual sections).

Quantification of the cone photoreceptor outer segment length

Retina sections (P15 and P21) were stained with rhodamine-conjugated peanut agglutinin to quantify the length of the cone photoreceptor outer segments. Representative sections from different animals (three animals per group) were counterstained and mounted with Vectashield Hard-Set Mounting Medium with DAPI (H1500, Vector Laboratories). Digital images were generated by a Leica epifluorescence microscope (DMRD), using the LAS AF v2.4.1 software. The ImageJ software v1.45 was used to quantify the length of the outer segments (n represents the number of individual outer segments measured).

Statistical analysis

Normality of the distribution was tested by the Kolmogorov–Smirnov test. Statistical analysis was performed using Student's t-test or the Mann–Whitney U test in case of a non-normal distribution. Values of $^{*}P < 0.05$, $^{**}P < 0.01$,

$^{***}P < 0.001$ were considered to be statistically significant. Values are expressed as means ± SEM. Calculations were made using the SPSS statistical package version 17.0.

SUPPLEMENTARY MATERIAL

Supplementary Material is available at *HMG* online.

ACKNOWLEDGEMENTS

The authors thank Marian Verhage for blastocyst injections, and Inge Versteeg, Rogier Vos, Christine Brussel, Fadime Üzel, Gudrun Utz and Pia Lacroix for technical assistance. The authors also thank all members of the Neuromedical Genetics group for advice on the manuscript.

Conflict of Interest statement. None declared.

FUNDING

This work was supported by Rotterdamse Vereniging Blindenbelangen, Landelijke St. voor Blinden en Slechtzienden, St. Blindenhulp, St. Oogfonds Nederland, St. Retina Nederland and Netherlands Institute for Neuroscience (J.W.), The Netherlands Organisation for Health Research and Development (ZonMw 43200004 to J.W.), European Union (HEALTH F2-2008-200234 to A.L.B., M.W.S., P.R., J.W.), The Deutsche Forschungsgemeinschaft (DFG Se837/5-2, Se837/6-1, Se837/6-2, Se837/7-1 to M.W.S.), the German Ministry of Education and Research (BMBF 0314106 to M.W.S.) and The French National Research Agency (ANR) (BLAN 07-2-186738 to A.L.B.).

REFERENCES

1. Mehalow, A.K., Kameya, S., Smith, R.S., Hawes, N.L., Denegre, J.M., Young, J.A., Bechtold, L., Haider, N.B., Tepass, U., Heckenlively, J.R. *et al.* (2003) CRB1 is essential for external limiting membrane integrity and photoreceptor morphogenesis in the mammalian retina. *Hum. Mol. Genet.*, **12**, 2179–2189.
2. van de Pavert, S.A., Kantardzhieva, A., Malysheva, A., Meuleman, J., Versteeg, I., Levelt, C., Klooster, J., Geiger, S., Seeliger, M.W., Rashbass, P. *et al.* (2004) Crumbs homologue 1 is required for maintenance of photoreceptor cell polarization and adhesion during light exposure. *J. Cell Sci.*, **117**, 4169–4177.
3. van de Pavert, S.A., Sanz, A.S., Aartsen, W.M., Vos, R.M., Versteeg, I., Beck, S.C., Klooster, J., Seeliger, M.W. and Wijnholds, J. (2007) Crb1 is a determinant of retinal apical Muller glia cell features. *Glia*, **55**, 1486–1497.
4. Park, B., Alves, C.H., Lundvig, D.M., Tanimoto, N., Beck, S.C., Huber, G., Richard, F., Klooster, J., Andlauer, T.F., Swindell, E.C. *et al.* (2011) PALS1 is essential for retinal pigment epithelium structure and neural retina stratification. *J. Neurosci.*, **31**, 17230–17241.
5. Sottocornola, R., Royer, C., Vives, V., Tordella, L., Zhong, S., Wang, Y., Ratnayaka, I., Shipman, M., Cheung, A., Gaston-Massuet, C. *et al.* (2010) ASPP2 binds Par-3 and controls the polarity and proliferation of neural progenitors during CNS development. *Dev. Cell*, **19**, 126–137.
6. Cho, S.H., Kim, J.Y., Simons, D.L., Song, J.Y., Le, J.H., Swindell, E.C., Jamrich, M., Wu, S.M. and Kim, S. (2012) Genetic ablation of Pals1 in retinal progenitor cells models the retinal pathology of Leber congenital amaurosis. *Hum. Mol. Genet.*, **21**, 2663–2676.
7. Koike, C., Nishida, A., Akimoto, K., Nakaya, M.A., Noda, T., Ohno, S. and Furukawa, T. (2005) Function of atypical protein kinase C lambda in differentiating photoreceptors is required for proper lamination of mouse retina. *J. Neurosci.*, **25**, 10290–10298.
8. van de Pavert, S.A., Meuleman, J., Malysheva, A., Aartsen, W.M., Versteeg, I., Tonagel, F., Kamphuis, W., McCabe, C.J., Seeliger, M.W. and Wijnholds, J. (2007) A single amino acid substitution (Cys249Trp) in Crb1 causes retinal degeneration and deregulates expression of pituitary tumor transforming gene Pttg1. *J. Neurosci.*, **27**, 564–573.
9. Pellikka, M., Tanentzapf, G., Pinto, M., Smith, C., McGlade, C.J., Ready, D.F. and Tepass, U. (2002) Crumbs, the *Drosophila* homologue of human CRB1/RP12, is essential for photoreceptor morphogenesis. *Nature*, **416**, 143–149.
10. Richard, M., Roepman, R., Aartsen, W.M., van Rossum, A.G., den Hollander, A.I., Knust, E., Wijnholds, J. and Cremers, F.P. (2006) Towards understanding CRUMBS function in retinal dystrophies. *Hum. Mol. Genet.*, **15**, 235–243.
11. Omori, Y. and Malicki, J. (2006) oko meduzy and related crumbs genes are determinants of apical cell features in the vertebrate embryo. *Curr. Biol.*, **16**, 945–957.
12. Hsu, Y.C. and Jensen, A.M. (2010) Multiple domains in the Crumbs Homolog 2a (Crb2a) protein are required for regulating rod photoreceptor size. *BMC Cell Biol.*, **11**, 60.
13. Tepass, U., Theres, C. and Knust, E. (1990) crumbs encodes an EGF-like protein expressed on apical membranes of *Drosophila* epithelial cells and required for organization of epithelia. *Cell*, **61**, 787–799.
14. Bulgakova, N.A. and Knust, E. (2009) The Crumbs complex: from epithelial-cell polarity to retinal degeneration. *J. Cell Sci.*, **122**, 2587–2596.
15. Kantardzhieva, A., Gosens, I., Alexeeva, S., Punte, I.M., Versteeg, I., Krieger, E., Neefjes-Mol, C.A., den Hollander, A.I., Letteboer, S.J., Klooster, J. *et al.* (2005) MPP5 recruits MPP4 to the CRB1 complex in photoreceptors. *Invest. Ophthalmol. Vis. Sci.*, **46**, 2192–2201.
16. Kantardzhieva, A., Alexeeva, S., Versteeg, I. and Wijnholds, J. (2006) MPP3 is recruited to the MPP5 protein scaffold at the retinal outer limiting membrane. *FEBS J.*, **273**, 1152–1165.
17. Assemat, E., Bazellieres, E., Pallesi-Pocachard, E., Le Bivic, A. and Massey-Harroche, D. (2008) Polarity complex proteins. *Biochim. Biophys. Acta*, **1778**, 614–630.
18. Roh, M.H., Makarova, O., Liu, C.J., Shin, K., Lee, S., Laurinec, S., Goyal, M., Wiggins, R. and Margolis, B. (2002) The Maguk protein, Pals1, functions as an adapter, linking mammalian homologues of Crumbs and Discs Lost. *J. Cell Biol.*, **157**, 161–172.
19. Lemmers, C., Michel, D., Lane-Guermonprez, L., Delgrossi, M.H., Medina, E., Arsanto, J.P. and Le Bivic, A. (2004) CRB3 binds directly to Par6 and regulates the morphogenesis of the tight junctions in mammalian epithelial cells. *Mol. Biol. Cell*, **15**, 1324–1333.
20. Hurd, T.W., Gao, L., Roh, M.H., Macara, I.G. and Margolis, B. (2003) Direct interaction of two polarity complexes implicated in epithelial tight junction assembly. *Nat. Cell Biol.*, **5**, 137–142.
21. Hsu, Y.C., Willoughby, J.J., Christensen, A.K. and Jensen, A.M. (2006) Mosaic Eyes is a novel component of the Crumbs complex and negatively regulates photoreceptor apical size. *Development*, **133**, 4849–4859.
22. Gosens, I., Sessa, A., den Hollander, A.I., Letteboer, S.J., Belloni, V., Arends, M.L., Le Bivic, A., Cremers, F.P., Broccoli, V. and Roepman, R. (2007) FERM protein EPB41L5 is a novel member of the mammalian CRB-MPP5 polarity complex. *Exp. Cell Res.*, **313**, 3959–3970.
23. Laprise, P., Beronja, S., Silva-Gagliardi, N.F., Pellikka, M., Jensen, A.M., McGlade, C.J. and Tepass, U. (2006) The FERM protein Yurt is a negative regulatory component of the Crumbs complex that controls epithelial polarity and apical membrane size. *Dev. Cell*, **11**, 363–374.
24. den Hollander, A.I., ten Brink, J.B., de Kok, Y.J., van Soest, S., van den Born, L.I., van Driel, M.A., van de Pol, D.J., Payne, A.M., Bhattacharya, S.S., Kellner, U. *et al.* (1999) Mutations in a human homologue of *Drosophila* crumbs cause retinitis pigmentosa (RP12). *Nat. Genet.*, **23**, 217–221.
25. den Hollander, A.I., Davis, J., van der Velde-Visser, S.D., Zonneveld, M.N., Pierrottet, C.O., Koenekoop, R.K., Kellner, U., van den Born, L.I., Heckenlively, J.R., Hoyng, C.B. *et al.* (2004) CRB1 mutation spectrum in inherited retinal dystrophies. *Hum. Mutat.*, **24**, 355–369.
26. Malicki, J. and Driever, W. (1999) oko meduzy mutations affect neuronal patterning in the zebrafish retina and reveal cell-cell interactions of the retinal neuroepithelial sheet. *Development*, **126**, 1235–1246.

27. Boroviak, T. and Rashbass, P. (2011) The apical polarity determinant Crumbs 2 is a novel regulator of ESC-derived neural progenitors. *Stem Cells*, **29**, 193–205.
28. Rowan, S. and Cepko, C.L. (2004) Genetic analysis of the homeodomain transcription factor Chx10 in the retina using a novel multifunctional BAC transgenic mouse reporter. *Dev. Biol.*, **271**, 388–402.
29. Schmitz-Valckenberg, S., Holz, F.G., Bird, A.C. and Spaide, R.F. (2008) Fundus autofluorescence imaging: review and perspectives. *Retina*, **28**, 385–409.
30. van Rossum, A.G., Aartsen, W.M., Meuleman, J., Klooster, J., Malysheva, A., Versteeg, I., Arsanto, J.P., Le Bivic, A. and Wijnholds, J. (2006) Pals1/Mpp5 is required for correct localization of Crb1 at the subapical region in polarized Muller glia cells. *Hum. Mol. Genet.*, **15**, 2659–2672.
31. Agathocleous, M. and Harris, W.A. (2009) From progenitors to differentiated cells in the vertebrate retina. *Annu. Rev. Cell Dev. Biol.*, **25**, 45–69.
32. Cepko, C.L., Austin, C.P., Yang, X., Alexiades, M. and Ezzeddine, D. (1996) Cell fate determination in the vertebrate retina. *Proc. Natl Acad. Sci. USA*, **93**, 589–595.
33. Ohata, S., Aoki, R., Kinoshita, S., Yamaguchi, M., Tsuruoka-Kinoshita, S., Tanaka, H., Wada, H., Watabe, S., Tsuboi, T., Masai, I. *et al.* (2011) Dual roles of Notch in regulation of apically restricted mitosis and apicobasal polarity of neuroepithelial cells. *Neuron*, **69**, 215–230.
34. Jacobson, S.G., Cideciyan, A.V., Aleman, T.S., Pianta, M.J., Sumaroka, A., Schwartz, S.B., Smilko, E.E., Milam, A.H., Sheffield, V.C. and Stone, E.M. (2003) Crumbs homolog 1 (CRB1) mutations result in a thick human retina with abnormal lamination. *Hum. Mol. Genet.*, **12**, 1073–1078.
35. Aleman, T.S., Cideciyan, A.V., Aguirre, G.K., Huang, W.C., Mullins, C.L., Roman, A.J., Sumaroka, A., Olivares, M.B., Tsai, F.F., Schwartz, S.B. *et al.* (2011) Human CRB1-associated retinal degeneration: comparison with the rd8 Crb1-mutant mouse model. *Invest. Ophthalmol. Vis. Sci.*, **52**, 6898–6910.
36. van den Hurk, J.A., Rashbass, P., Roepman, R., Davis, J., Voesenek, K.E., Arends, M.L., Zonneveld, M.N., van Roekel, M.H., Cameron, K., Rohrschneider, K. *et al.* (2005) Characterization of the Crumbs homolog 2 (CRB2) gene and analysis of its role in retinitis pigmentosa and Leber congenital amaurosis. *Mol. Vis.*, **11**, 263–273.
37. Warming, S., Costantino, N., Court, D.L., Jenkins, N.A. and Copeland, N.G. (2005) Simple and highly efficient BAC recombineering using galK selection. *Nucleic Acids Res.*, **33**, e36.
38. Tanimoto, N., Muehlfriedel, R.L., Fischer, M.D., Fahl, E., Humphries, P., Biel, M. and Seeliger, M.W. (2009) Vision tests in the mouse: functional phenotyping with electroretinography. *Front. Biosci.*, **14**, 2730–2737.
39. Seeliger, M.W., Beck, S.C., Pereyra-Munoz, N., Dangel, S., Tsai, J.Y., Luhmann, U.F., van de Pavert, S.A., Wijnholds, J., Samardzija, M., Wenzel, A. *et al.* (2005) In vivo confocal imaging of the retina in animal models using scanning laser ophthalmoscopy. *Vision Res.*, **45**, 3512–3519.
40. Fischer, M.D., Huber, G., Beck, S.C., Tanimoto, N., Muehlfriedel, R., Fahl, E., Grimm, C., Wenzel, A., Reme, C.E., van de Pavert, S.A. *et al.* (2009) Noninvasive, in vivo assessment of mouse retinal structure using optical coherence tomography. *PloS One*, **4**, e7507.